

Functional Transform-Based Low-Rank Tensor Factorization for Multi-Dimensional Data Recovery

Jianli Wang¹ and Xile Zhao²

¹ Southwest Jiaotong University, Chengdu, China
wangjianli_123@163.com

² University of Electronic Science and Technology of China, Chengdu, China
xlzhao122003@163.com

Abstract. Recently, the transform-based low-rank tensor factorization (t-LRTF) has emerged as a promising tool for multi-dimensional data recovery. However, the discrete transforms along the third (*i.e.*, temporal/spectral) dimension are dominating in existing t-LRTF methods, which hinders their performance in addressing temporal/spectral degeneration scenarios, *e.g.*, video frame interpolation and multispectral image (MSI) spectral super-resolution. To overcome this barrier, we propose a Functional Transform-based Low-Rank Tensor Factorization (FLRTF), where the learnable functional transform is expressed by the implicit neural representation with positional encodings. The continuity brought by this function allows FLRTF to capture the smoothness of data in the third dimension, which will benefit the recovery of temporal/spectral degeneration problems. To examine the effectiveness of FLRTF, we establish a general FLRTF-based multi-dimensional data recovery model. Experimental results, including video frame interpolation/extrapolation, MSI band interpolation, and MSI spectral super-resolution tasks, substantiate that FLRTF has superior performance as compared with representative data recovery methods.

Keywords: Functional transform · Implicit neural representation · Low-rank tensor factorization

1 Introduction

With the development of modern imaging systems, data with multiple dimensions (*e.g.*, color images [38, 39], videos [33], multispectral images (MSIs) [4, 44], network traffic data [5], and so on) are increasingly emerging. Real-world multi-dimensional data are naturally represented by tensors [42] as they can deliver the underlying information of data more faithfully and accurately than vector/matrix formats. Consequently, tensor modeling technique have gained popularity in multi-dimensional data processing and representation [17, 41].

Owing to the fact that multi-dimensional data often exhibit strong global correlation [1, 23], which can be mathematically represented as a low-rank property, low-rank tensor modeling has prompted extensive research. This approach

is pivotal for the recovery and analysis of multi-dimensional data. Distinct from the matrix case, the concept of tensor rank is not unequivocal [11, 32]. The most well-known tensor ranks include CANDECOMP/PARAFAC (CP) rank [40, 48], Tucker rank [23, 24, 36], and tensor tubal-rank [12, 16, 50]. Additionally, recent literature has introduced new tensor ranks based on tensor network decomposition, including the tensor train rank [7, 46], tensor ring rank [45, 47], and fully connected tensor network rank [52, 53]. This paper specifically focuses on the tensor tubal-rank [12, 16, 21].

Attributed to the beautiful algebraic property, the tensor singular value decomposition (t-SVD) [25, 43] has garnered great interest in addressing multi-dimensional data recovery. [20, 26]. Initially introduced by Braman *et al.* [2], t-SVD allows for the decomposition of any third-order tensor into the tensor-tensor product (t-product) of two orthogonal tensors and a f -diagonal tensor. Based on t-SVD, a novel definition of tensor rank, termed tensor tubal-rank, has been presented. This rank is numerically defined as number of non-zero tubes within the f -diagonal tensor resulting from t-SVD [49]. Given that the computational complexity of minimizing the tensor tubal-rank, which is an NP-hard problem, Zhang *et al.* [49] introduced the tensor nuclear norm (TNN), which serves as a convex surrogate for the tensor tubal-rank and has been applied to the tensor completion problem.

The choice of transform is crucial in the TNN, as it operates on the third mode of the tensor to convert it into a low-rank representation. A few variations of TNN employing different transforms have been explored in the literatures. For instance, Madathil *et al.* [30] adopted the real-valued discrete cosine transform instead of the original discrete Fourier transform (DFT) in the t-SVD framework to mitigate the computational burden arising from complex operations. More generally, Lu *et al.* [26] established a novel tensor tubal-rank through the invertible linear transform and offered the theoretically sampling bound to guarantee the exact recovery. In contrast to traditional invertible transforms, Jiang *et al.* [14] introduced a non-invertible framelet transform in t-SVD for addressing the third-order tensor completion problem. Furthermore, Jiang and Kong *et al.* [15, 20] introduced some data-driven transforms in the t-SVD framework that exhibits superior and more adaptable expressive capabilities compared to pre-defined transforms. In [27], Luo *et al.* suggested a novel TNN based on the nonlinear transform, which is learned through a self-supervised multi-layer neural network. To reduce computational overhead and efficiently handle large scale data, Zhou *et al.* [54] employed the low-tubal-rank tensor factorization (LRTF) to preserve the low-tubal-rank property of the data and presented a new tensor completion model. More recently, Luo *et al.* [29] proposed a hierarchical LRTF for multi-dimensional data recovery, where the multilayer perceptron is used as a nonlinear transform in the t-SVD framework. Despite these advancements, these methods usually considers a discrete transform, which reflects sparse samples of the spectral/temporal signature. This limitation constrains their effectiveness and adaptability in addressing temporal/spectral degeneration scenarios, such

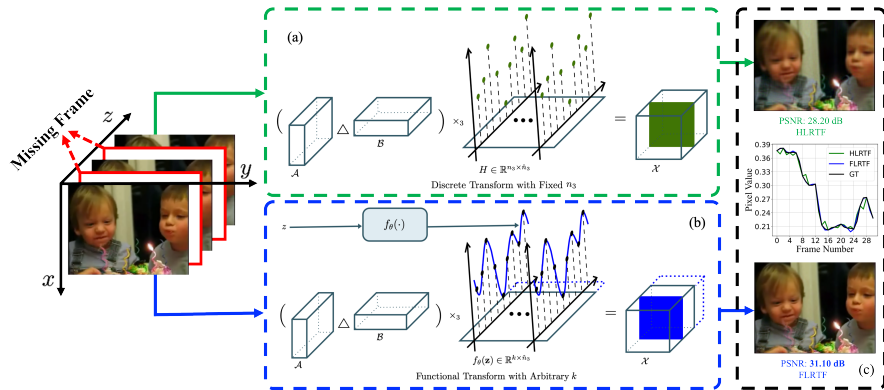


Fig. 1: An illustration of the proposed FLRTF. (a) An example of the discrete transform-based low-rank tensor factorization, *e.g.*, HLRTF [29]. (b) The proposed functional transform-based low-rank tensor factorization, *i.e.*, FLRTF. (c) Result examples on video frame interpolation task for different methods.

as video frame interpolation [3,6] and MSI spectral super-resolution [8,9,31]; an example is shown in Fig. 1.

In this work, we propose a pioneering approach called **F**unctional transform-based **L**ow-**R**ank **T**ensor **F**actorization (FLRTF) for multi-dimensional data recovery. To the best of our knowledge, this is the first attempt to employ a functional transform along the third dimension in the t-SVD framework. More specifically, we use the implicit neural representations with positional encodings, which is expressed by a continuous coordinate-based implicit function, to learn the functional transform. The continuity brought by this function allows the proposed FLRTF captures the local smoothness of multi-dimensional data in the third dimension, which is beneficial for the multi-dimensional data recovery, especially in the temporal/spectral degeneration scenarios. Additionally, we employ multilayer perceptron (MLP) with the powerful approximation capability to parameterize this implicit function, enhancing FLRTF’s ability to faithfully capture intricate details of data. To validate the efficacy of the proposed FLRTF, we establish a general FLRTF-based model for multi-dimensional data recovery. We compare the performance of discrete transform-based LRTF methods, such as HLRTF [29] with the functional transform-based LRTF method (*i.e.*, the proposed FLRTF) using the *Blowing Candles* dataset under the video frame interpolation task in Fig. 1. The results indicate that HLRTF [29] (*i.e.*, the discrete transform-based LRTF method) demonstrates suboptimal recovery performance. In contrast, FLRTF yields clearer spatial details and textures compared to HLRTF. In addition, the proposed FLRTF enhances the performance of HLRTF by up to 2.9 dB in terms of peak signal-to-noise ratio (PSNR), which also indicates its superior recovery capability.

In general, the main contributions of this work can be encapsulated in the following three aspects:

(i) We present a pioneering functional transform-based low-rank tensor factorization, termed as FLRTF. To the best of our knowledge, this is the first attempt to employ a functional transform along the third dimension in the t-SVD framework. Notably, FLRTF can simultaneously capture the local smoothness of data in the spectral/temporal dimension and the global low-rankness. This dual capability reveals FLRTF’s potential effectiveness in the multi-dimensional data recovery, especially in the temporal/spectral degeneration scenarios.

(ii) We leverage the implicit neural representations with positional encodings, which are parameterized by MLP, to learn the functional transform. The continuity of this functional transform, coupled with the powerful approximation capability of MLP, allows FLRTF to continuously represent data in the spectral/temporal dimension and effectively capture intricate details of data.

(iii) Building upon the proposed FLRTF, we formulate a general FLRTF-based multi-dimensional data recovery model. Extensive experimental results, including video frame synthesis, MSI band interpolation, and MSI spectral super-resolution tasks, validate the superior performance of the proposed FLRTF over representative multi-dimensional data recovery methods, especially in spectral/temporal fidelity. This shows its wide applicability and effectiveness in various scenarios.

2 Notations

We employ calligraphic capital letters, *e.g.*, \mathcal{A} , boldface capital letters, *e.g.*, \mathbf{A} , boldface lowercase letters, *e.g.*, \mathbf{a} , and lowercase letters, *e.g.*, a , to represent tensors, matrices, vectors, and scalars, respectively. The i -th element of a vector \mathbf{a} is denoted by a_i . For a tensor $\mathcal{A} \in \mathbb{R}^{n_1 \times n_2 \times n_3}$, the i -th frontal slice is defined as $\mathcal{A}^{(i)} \in \mathbb{R}^{n_1 \times n_2}$ or $\mathcal{A}(:, :, i) \in \mathbb{R}^{n_1 \times n_2}$, and the (i, j, k) -th element is represented as $a_{i,j,k}$ or $\mathcal{A}(i, j, k)$. The Frobenius norm of \mathcal{A} is given by $\|\mathcal{A}\|_F = \sqrt{\sum_{i,j,k} |a_{i,j,k}|^2}$, and the ℓ_1 -norm of \mathcal{A} is defined by $\|\mathcal{A}\|_{\ell_1} = \sum_{i,j,k} |a_{i,j,k}|$. The face-wise product of $\mathcal{A} \in \mathbb{R}^{n_1 \times n_2 \times n_3}$ and $\mathcal{B} \in \mathbb{R}^{n_2 \times n_4 \times n_3}$ is defined as matrix products for all frontal slices of two tensors [17], *i.e.*, $\mathcal{X} = \mathcal{A} \triangle \mathcal{B} \in \mathbb{R}^{n_1 \times n_4 \times n_3}$, where the i -th frontal slice of \mathcal{X} is $\mathcal{A}^{(i)} \mathcal{B}^{(i)}$ ($i = 1, \dots, n_3$). Leveraging the face-wise product, the t-product is established as the face-wise product of two tensors after DFT.

Definition 1. (*Mode-3 unfolding and folding [19]*) For a tensor $\mathcal{A} \in \mathbb{R}^{n_1 \times n_2 \times n_3}$, its mode-3 unfolding, represented as $\mathbf{A}_{(3)} \in \mathbb{R}^{n_3 \times n_1 n_2}$, is a matrix that maps elements from the tensor to the matrix such that $\mathbf{A}_{(3)}(k, l)$ corresponds to $\mathcal{A}(i, j, k)$, where $l = (j - 1)n_1 + i$. The mode-3 unfolding and folding operators are denoted by $\mathbf{A}_{(3)} = \mathbf{Unfold}_3(\mathcal{A})$ and $\mathcal{A} = \mathbf{Fold}_3(\mathbf{A}_{(3)})$, respectively.

Definition 2. (*Tensor-matrix product [19]*) The tensor-matrix product between $\mathcal{A} \in \mathbb{R}^{n_1 \times n_2 \times n_3}$ and $\mathbf{F} \in \mathbb{R}^{J \times n_3}$ is defined as $\mathcal{A} \times_3 \mathbf{F} = \mathbf{Fold}_3(\mathbf{F} \mathbf{Unfold}_3(\mathcal{A}))$.

Theorem 1. (*Low-rank tensor factorization [29]*) For a third-order tensor $\mathcal{X} \in \mathbb{R}^{n_1 \times n_2 \times n_3}$, there exist two tensors $\mathcal{A} \in \mathbb{R}^{n_1 \times r \times \hat{n}_3}$ and $\mathcal{B} \in \mathbb{R}^{r \times n_2 \times \hat{n}_3}$, and a

transform $\mathfrak{L} : \mathbb{R}^{1 \times 1 \times \hat{n}_3} \rightarrow \mathbb{R}^{1 \times 1 \times n_3}$ such that the following equation holds:

$$\mathcal{X} = (\mathcal{A} \triangle \mathcal{B}) \times_3 \mathbf{L},$$

where $\mathbf{L} \in \mathbb{R}^{n_3 \times \hat{n}_3}$ represents the transform matrix corresponding to \mathfrak{L} .

3 The Proposed Method

3.1 The Proposed FLRTF

Recently, the t-LRTF has emerged as a promising tool for multi-dimensional data recovery. However, the performance of existing t-LRTF methods that consider discrete transforms is unsatisfactory in addressing temporal/spectral degeneration scenarios, *e.g.*, video frame interpolation and MSI spectral super-resolution. To handle these challenging temporal/spectral degeneration scenarios, we propose a pioneering functional transform-based low-rank tensor factorization, which allows us to simultaneously exploit the local smoothness of data in the third dimension and its inherent low-rankness.

Definition 3. (*Functional transform-based low-rank tensor factorization*) Given a third-order tensor $\mathcal{X} \in \mathbb{R}^{n_1 \times n_2 \times n_3}$, we define its FLRTF representation form by using two factor tensors $\mathcal{A} \in \mathbb{R}^{n_1 \times r \times \hat{n}_3}$ and $\mathcal{B} \in \mathbb{R}^{r \times n_2 \times \hat{n}_3}$, and a functional transform $f(\cdot) : D_f \rightarrow \mathbb{R}^{\hat{n}_3}$, where $D_f = (0, 1]$ represents the definition domain. The k -th frontal slice of \mathcal{X} is defined as

$$\mathcal{X}(:, :, k) := (\mathcal{A} \triangle \mathcal{B}) \times_3 f(\mathbf{z}_{(k)}), k = 1, 2, \dots, n_3,$$

where $\mathbf{z} = [\frac{1}{n_3}, \frac{2}{n_3}, \dots, \frac{n_3}{n_3}]$ represents the sampling coordinate vector.

Note that the proposed FLRTF can degrade into the classical low-rank tensor factorization (see **Theorem 1**), when the definition domain D_f is a discrete set of some constants, *e.g.*, $D_f = \{1, 2, \dots, n_3\}$.

Functional transform: The functional transform is utilized to exploit the continuity characteristic of data in the third (*i.e.*, temporal/spectral) dimension. In our work, we employ MLPs to parameterize the functional transform $f(\cdot)$ due to its powerful universal approximation capability, which allows for more flexible representation learning compared to predefined function transform. Specifically, the implicit functional transform can be formulated as

$$f_\theta(\mathbf{x}) = \mathbf{H}_l(\sigma(\mathbf{H}_{l-1} \cdots \sigma(\mathbf{H}_1 \mathbf{x}))) : D_f \rightarrow \mathbb{R}^{\hat{n}_3}, \quad (1)$$

where \mathbf{x} represents the sampling coordinate of the third dimension, $\theta := \{\mathbf{H}_i\}_{i=1}^l$ are learnable weights of the MLP, and $\sigma(\cdot)$ is the nonlinear activation function.

Remark. In contrast to existing t-LRTF methods, the advantage of the proposed FLRTF is that we employ a continuous implicit neural representation to learn a functional transform within the LRTF framework. As far as we are aware, this is the first attempt to employ a functional transform along the third

dimension in the t-SVD framework. The continuity brought by this functional transform allows the proposed FLRTF to not only capture the low-rankness of data but also the local smoothness of its third dimension, which is beneficial for data recovery, especially in temporal/spectral degradation scenarios.

Next, we theoretically justify that the proposed FLRTF can encode the local smoothness of data in the third dimension.

Theorem 2. *Let $\mathcal{A} \in \mathbb{R}^{n_1 \times r \times \hat{n}_3}$, $\mathcal{B} \in \mathbb{R}^{r \times n_2 \times \hat{n}_3}$, and $f_\theta(\cdot) : D_f \rightarrow \mathbb{R}^{\hat{n}_3}$ be the MLP structured as in (1) with parameters θ , where $D_f = (0, 1]$ represents the definition domain. Suppose that*

- $\sigma(\cdot)$ exhibits Lipschitz continuous with Lipschitz constant δ .
- $\|\mathcal{A}\|_{\ell_1}$ is bounded by γ_1 and $\|\mathcal{B}\|_{\ell_1}$ is bounded by γ_2 .
- For any weight matrix \mathbf{H}_i in the MLP, $\|\mathbf{H}_i\|_{\ell_1}$ is bounded by γ_3 .

Define a third-order tensor $\mathcal{X} \in \mathbb{R}^{n_1 \times n_2 \times n_3}$ that satisfies its k -th frontal slice is given by $\mathcal{X}(:, :, k) := (\mathcal{A} \Delta \mathcal{B}) \times_3 f(\mathbf{z}_{(k)})$, $k = 1, 2, \dots, n_3$, where $\mathbf{z} = [\frac{1}{n_3}, \frac{2}{n_3}, \dots, \frac{n_3}{n_3}]$ represents the sampling coordinate vector. Then, there exists a constant $\frac{\gamma_1 \gamma_2 \gamma_3^l \delta^{l-1}}{n_3} > 0$ such that the following inequality holds:

$$\|\mathcal{X}(i, j, k) - \mathcal{X}(i, j, k-1)\|_{\ell_1} \leq \frac{\gamma_1 \gamma_2 \gamma_3^l \delta^{l-1}}{n_3}.$$

where $i = 1, 2, \dots, n_1$, $j = 1, 2, \dots, n_2$, and $k = 1, 2, \dots, n_3$. Please refer to the supplementary material for the detailed proof³.

Theorem 2 implies that for the sampled tensor \mathcal{X} , the difference between its adjacent elements in third dimension is bounded by a constant $\frac{\gamma_1 \gamma_2 \gamma_3^l \delta^{l-1}}{n_3}$. Consequently, the proposed FLRTF implicitly and efficiently unifies the low-rankness and smoothness. The dual capability of the proposed FLRTF reveals its potential effectiveness in the multi-dimensional data recovery, especially in the temporal/spectral degeneration scenarios.

3.2 FLRTF for Multi-Dimensional Data Recovery

To examine the effectiveness of the proposed FLRTF, we propose a general FLRTF-based multi-dimensional data recovery model. Given an observed multi-dimensional data $\mathcal{O} \in \mathbb{R}^{n_1 \times n_2 \times b}$, the proposed FLRTF-based multi-dimensional data recovery model can be formulated as follows:

$$\min_{\mathcal{A}, \mathcal{B}, \theta} \ell(\mathcal{O}, \mathcal{X}), \quad \text{s.t. } \mathcal{X}(:, :, k) = (\mathcal{A} \Delta \mathcal{B}) \times_3 f_\theta(\mathbf{z}_{(k)}), \quad (2)$$

where $\mathcal{A} \in \mathbb{R}^{n_1 \times r \times \hat{n}_3}$ and $\mathcal{B} \in \mathbb{R}^{r \times n_2 \times \hat{n}_3}$ are two latent factor tensors, $f_\theta(\cdot) : D_f \rightarrow \mathbb{R}^{\hat{n}_3}$ is the implicit neural representation function parameterized by the MLP with parameters θ , $\mathbf{z} = [\frac{1}{n_3}, \frac{2}{n_3}, \dots, \frac{n_3}{n_3}]$ represents the sampling coordinate

³ <https://wangjianli123.github.io/homepage/>

vector, and $k = 1, 2, \dots, n_3$. $\ell(\cdot, \cdot)$ denotes the data fidelity item that guarantees the solution accords with degradation, which can be flexibly adjusted for different tasks. Note that the proposed model (2) is supervised and solely requires the observed data without a training dataset. Therefore, it can be flexibly applied to different datasets and degradation conditions.

In this work, we first consider two temporal/spectral degeneration tasks, *i.e.*, video frame synthesis and MSI band interpolation. Subsequently, we explore the potential of the proposed FLRTF in the general spectral degradation task with a degenerate operator, *i.e.*, MSI spectral super-resolution. For these three temporal/spectral degradation tasks, the proposed FLRTF-based multi-dimensional data recovery model (2) can be represented in unified manner as follows:

$$\min_{\mathcal{A}, \mathcal{B}, \theta} \|\mathcal{O} - \mathcal{X} \times_3 \mathbf{W}\|_F^2, \quad \text{s.t. } \mathcal{X}(:, :, k) = (\mathcal{A} \triangle \mathcal{B}) \times_3 f_\theta(\mathbf{z}_{(k)}), \quad (3)$$

where \mathbf{W} is a task-related weight matrix. Next, we introduce these three tasks.

- **Video Frame Synthesis:** Video frame synthesis (VFS) aims at constructing new video frames from an existing video, which can be broadly categorized into two types, *i.e.*, interpolation and extrapolation. It has found wide applications in practice, such as slow-motion video creation [13] and animation production [37]. In fact, VFS can be viewed as a tensor completion problem with randomly frontal slice missing, the corresponding weight matrix is a square matrix. The (i, j) -th element of $\mathbf{W} \in \mathbb{R}^{n_3 \times n_3}$ is defined as

$$w_{i,j} = \begin{cases} 1, & \text{if } i \in \Omega_c \text{ and } i = j, \\ 0, & \text{otherwise.} \end{cases} \quad (4)$$

where $\Omega \subseteq \{1, 2, \dots, n_3\}$ represents the index set of the missing frames, and Ω_c stands for the complementation of Ω .

- **MSI Band Interpolation:** MSIs play an important role in various applications. However, due to hardware constraints, it is not uncommon for MSI products to exhibit one or more missing bands [35], which diminishes the reliability of the information provided. MSI band interpolation/reconstruction (MBI) aims at recovering missing bands from the observation by leveraging information from the available bands. In fact, MBI is a tensor completion problem with randomly frontal slice missing, the corresponding weight matrix is a square matrix. The (i, j) -th element of $\mathbf{W} \in \mathbb{R}^{n_3 \times n_3}$ is defined as Eq. (4), where $\Omega \subseteq \{1, 2, \dots, n_3\}$ represents the index set of the missing bands.

- **MSI Spectral Super-Resolution:** MSI spectral super-resolution (MSSR) aims at recovering multispectral imaging from its spectrally downsampled measurement (*e.g.*, RGB images) [10], which is a crucial technique in computer vision. For MSSR task, the observed data $\mathcal{O} \in \mathbb{R}^{n_1 \times n_2 \times 3}$ and the corresponding weight matrix is a spectral response functions of RGB cameras, which is provided in advance.

In the proposed model (3), the optimization variables include factor tensors (*i.e.*, \mathcal{A} and \mathcal{B}) and the weights of the MLP. Given that the objective function is a squared error term, which is differentiable with respect to factor tensors

Algorithm 1 Adam-based solving algorithm of the proposed FLRTF for multi-dimensional data recovery.

Input: Observed data $\mathcal{O} \in \mathbb{R}^{n_1 \times n_2 \times b}$, the task-related weight matrix \mathbf{W} , parameters r and \hat{n}_3 ;

Initialization: Initialize factor tensors $\mathcal{A} \in \mathbb{R}^{n_1 \times r \times \hat{n}_3}$ and $\mathcal{B} \in \mathbb{R}^{r \times n_2 \times \hat{n}_3}$, and MLP weights θ ;

1: **for** $k = 1$ to k_{max} **do**

2: Compute the recovered data $\mathcal{X} \in \mathbb{R}^{n_1 \times n_2 \times n_3}$ via $\mathcal{X}(:, :, k) = (\mathcal{A} \triangle \mathcal{B}) \times_3 f_\theta(\mathbf{z}_{(k)})$ for $k = 1, 2, \dots, n_3$;

3: Compute the loss function in model (3) for different tasks;

4: Compute the gradients w.r.t. \mathcal{A} , \mathcal{B} , and θ ;

5: Update \mathcal{A} , \mathcal{B} , and θ using the Adam optimizer [18];

6: **end for**

Output: The recovered multi-dimensional data \mathcal{X} .

and all MLR weights, we can employ the adaptive moment estimation (Adam) optimizer [18] to address the model (3). Simultaneously, we set a maximum iteration number k_{max} as the stopping criterion for the Adam-based solving algorithm in our experiments. Once the optimal factor tensors and MLP weights are obtained by solving problem (3), the recovery result \mathcal{X} can be computed by $\mathcal{X}(:, :, k) = (\mathcal{A} \triangle \mathcal{B}) \times_3 f_\theta(\mathbf{z}_{(k)})$ for $k = 1, 2, \dots, n_3$. The pseudocode of the Adam-based solving algorithm for FLRTF is outlined in Algorithm 1.

4 Experiments

4.1 Experimental Settings

Parameter Settings. In the proposed FLRTF, the hyperparameters include the functional transform-based tubal-rank and the size of the factor tensors \mathcal{A} and \mathcal{B} in the third dimension, *i.e.*, r and \hat{n}_3 , respectively. These parameters are empirically chosen from the candidate sets $\{k\}_{k=1}^{30}$ and $\{kn_3\}_{k=1}^6$, respectively, to obtain the best performance. The learning rate for the Adam optimizer is selected from the candidate set $\{0.001, 0.003, 0.005\}$ to achieve optimal results. The maximum number of iterations and the number of layers in the MLP are fixed at 10000 and 5, respectively, for all tasks. For simplicity, the dimension of each layer, except the last, of the MLP is set to 64, and the last layer is set to \hat{n}_3 in our experiments. The nonlinear activation function selected for this study is the *sinusoidal* function, *i.e.*, $\sigma(\cdot) = \sin(\cdot)$. For comparative methods DCTNN [30], TNN-3DTV [34], HLRTF [29], and t-CTV [42], all parameters are manually adjusted according to the authors' default strategies in their papers to obtain optimal performance. For the comparison methods HRNet [51], GDNet [55], HSACS [22], HSRnet [9], and SSDCN [9], all codes are implemented with their recommended parameters.

Evaluation Indices. To quantitatively evaluate the overall quality of the recovered results obtained by different methods, several quantitative evaluation

Table 1: The computational complexity of various methods.

Methods	Computational complexity
DCTNN	$\mathcal{O}(n_1 n_2 n_3 \log n_3 + n_1 n_2 n_3 \min(n_1, n_2))$
TNN-3DTV	$\mathcal{O}(n_1 n_2 n_3 \log(n_1 n_2 n_3) + n_1 n_2 n_3 \min(n_1, n_2))$
HLRFT	$\mathcal{O}(n_1 n_2 \hat{n}_3 (m + r) + n_1 n_2 m^2 (l - 2) + n_1 n_2 n_3 m)$
t-CTV	$\mathcal{O}(n_1 n_2 n_3 \log(n_1 n_2 n_3) + n_1 n_2 n_3 \min(n_1, n_2))$
FLRFT	$\mathcal{O}(m^2 (l - 2) n_3 + n_1 n_2 \hat{n}_3 r + n_1 n_2 n_3 \hat{n}_3)$

indexes are used in our experiments. For video frame synthesis, we utilize the PSNR, the structural similarity (SSIM), and the universal image quality index (UIQI) as metrics. Higher PSNR, SSIM, and UIQI values correspond to superior performance. For the MSI band interpolation and MSI spectral super-resolution, we adopt the PSNR, the SSIM, and the spectral angle mapping (SAM) as evaluation indices. A lower SAM value corresponds to superior performance.

Experimental Platform. All experiments were conducted on the Windows 11 platform with an Intel Core i9-13900KF processor (3.00 GHz, 128 GB RAM) and an NVIDIA RTX 4090 GPU (12 GB GPU memory). Our method is implemented using PyTorch 2.0.0 with GPU calculation.

4.2 Datasets and Compared Methods

Video Frame Synthesis. VFS aims at constructing new video frames from an existing video, which can be categorized into two primary types, *i.e.*, interpolation and extrapolation. Video frame interpolation seeks to recover missing frames between given frames, while video frame extrapolation is to generate future frames based on historical frames. We employ four video clips from the *UCF-101* dataset⁴, which are widely used for VFS task, to evaluate the performance of the proposed FLRFT in our experiments, *w.*, *i.e.*, *Apply Eye Make-up*, *Blowing Candles*, *Writing On Board*, and *Typing*. The size of the top three data is $240 \times 176 \times 3 \times 31$ and the size of the last one data is $178 \times 238 \times 3 \times 31$. For video frame interpolation and extrapolation, the index set of missing frames are set as $\{2, 4, \dots, 30\}$ and $\{31\}$, respectively. To comprehensively evaluate the proposed FLRFT, we compare it with four state-of-the-art multi-dimensional data recovery methods, including DCTNN [30], TNN-3DTV [34], HLRFT [29], and t-CTV [42]. We select DCTNN since it represents the classic transform-based TNN method. We select HLRFT since it is the most relevant to the proposed FLRFT among the newer methods for multi-dimensional data recovery. We select TNN-3DTV and t-CTV since they simultaneously explore the local smoothness and global low-rankness of data. The computational complexity of different methods on $\mathcal{X} \in \mathbb{R}^{n_1 \times n_2 \times n_3}$ are shown in Table 1 for comparison, where r is the rank, \hat{n}_3 represents the size of factor tensor in the third dimension, m represents the number of hidden units of MLP, and l represents the number of layers.

⁴ <https://www.crcv.ucf.edu/research/data-sets/ucf101/>



Fig. 2: Visualization of recovery results by different methods for video frame interpolation and extrapolation tasks. From top to bottom: the 31 frame of *Apply Eye Make-up*, the 31 frame of *Writing On Board*, the 2 frame of *Blowing Candles*, and the 16 frame of *Typing*.

Table 2: Quantitative comparison of different methods for video frame interpolation and extrapolation tasks. The best and second-best values are highlighted in bold and underline, respectively.

Interpolation	<i>Apply Eye Make-up</i>	<i>Blowing Candles</i>	<i>Writing On Board</i>	<i>Typing</i>
DCTNN	13.78/0.549/0.349	18.39/0.459/0.360	21.19/0.790/0.467	20.97/0.695/0.690
TNN-3DTV	<u>31.41/0.954/0.774</u>	<u>30.20/0.914/0.781</u>	<u>28.09/0.932/0.818</u>	<u>28.47/0.923/0.935</u>
HLRTF	28.65/0.907/0.675	28.36/0.849/0.632	27.97/0.912/0.607	28.21/0.903/0.876
t-CTV	29.29/0.910/0.589	29.36/0.854/0.609	27.45/0.892/0.664	28.34/0.916/0.875
FLRTF	32.83/0.954/0.734	31.10/0.915/0.741	28.860/0.913/0.700	31.94/0.931/0.965
Extrapolation	<i>Apply Eye Make-up</i>	<i>Blowing Candles</i>	<i>Writing On Board</i>	<i>Typing</i>
DCTNN	20.19/0.749/0.486	23.03/0.697/0.450	22.74/0.806/0.523	27.13/0.873/0.784
TNN-3DTV	15.60/0.648/0.331	19.44/0.650/0.364	19.51/ <u>0.832/0.635</u>	24.04/0.863/0.760
HLRTF	<u>21.47/0.756/0.407</u>	<u>23.22/0.780/0.557</u>	24.52/0.853/0.596	<u>38.52/0.976/0.949</u>
t-CTV	15.62/0.647/0.340	19.55/0.637/0.354	19.73/0.829/0.560	24.19/0.859/0.756
FLRTF	22.80/0.802/0.532	23.57/0.785/0.579	<u>24.38/0.828/0.523</u>	40.29/0.986/0.964

MSI Band Interpolation. MBI aims at recovering missing bands from the observation by utilizing spectral information of the other bands. In our experiments, we utilize four MSIs from the *CAVE*⁵ dataset to evaluate the performance of the proposed FLRTF, including *Toy*, *Flowers*, *Jelly Beans*, and

⁵ <https://www1.cs.columbia.edu/CAVE/databases/multispectral/>

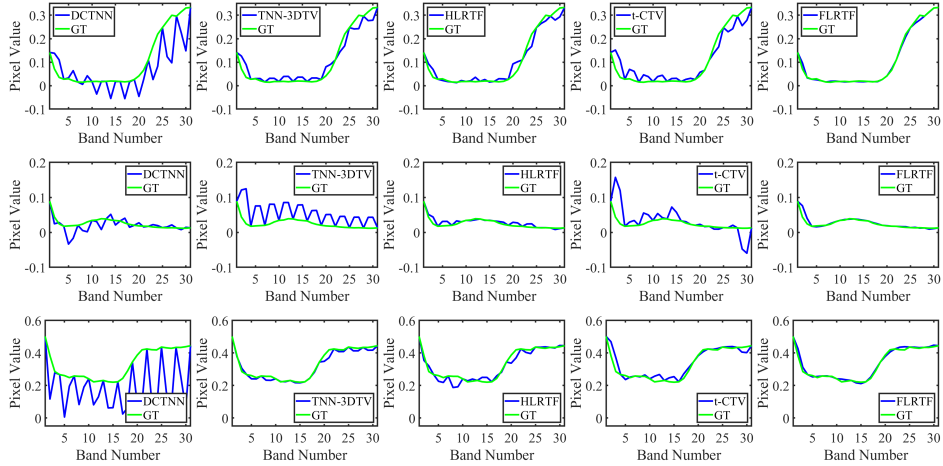


Fig. 3: Spectral curves of the recovered results by different methods for MBI task. From top to bottom: the results at spatial location (150, 150) in *Toy*, the results at spatial location (220, 100) in *Flowers*, and the results at spatial location (250, 100) in *Jelly Beans*, respectively.

Table 3: Quantitative comparison of different methods for MBI task. The best and second-best values are highlighted in bold and underline, respectively.

Data	<i>Toy</i>	<i>Flowers</i>	<i>Pompoms</i>	<i>Jelly Beans</i>
DCTNN	12.13/0.431/44.54	14.58/0.336/50.31	11.86/0.109/74.39	15.24/0.181/15.24
TNN-3DTV	30.26/0.928/30.26	31.77/ <u>0.918</u> / 12.86	32.49/0.924/ <u>8.391</u>	27.82/0.889/ <u>10.14</u>
HLRTF	<u>38.24</u> / <u>0.979</u> / <u>10.71</u>	<u>36.17</u> /0.911/15.19	<u>33.69</u> / <u>0.952</u> /10.37	<u>33.21</u> / <u>0.917</u> /13.82
t-CTV	36.58/0.935/16.76	33.66/0.805/25.37	27.78/0.852/18.69	32.28/0.858/20.29
FLRTF	43.22 / 0.992 / 7.755	44.13 / 0.970 / <u>14.35</u>	40.19 / 0.990 / 6.375	42.47 / 0.987 / 7.599

Pompoms. The original size of these datasets is $512 \times 512 \times 31$, and we resize them into $256 \times 256 \times 31$ for our experiments. The index set of missing bands is set as $\{2, 3, 5, 6, \dots, 29, 30\}$. Similar to VFS task, we select DCTNN [30], TNN-3DTV [34], HLRTF [29], and t-CTV [42] as the comparing methods.

MSI Spectral Super-Resolution. MSSR aims at recovering multispectral imaging from its spectrally downsampled measurement (*e.g.*, RGB images). In our experiments, we conduct spectral recovery based on RGB-to-MSI mapping, and employ *CAVE* and *ARAD_1K* provided by *New Trends in Image Restoration and Enhancement* workshop (NTIRE 2022⁶) datasets to evaluate the performance of the proposed FLRTF. For *CAVE* dataset, which covers the wavelength range from 400 nm to 700 nm and contains 32 scenarios, we select all MSIs as testing data. The original size of these datasets is $512 \times 512 \times 31$ and

⁶ <https://codalab.lisn.upsaclay.fr/competitions/721>

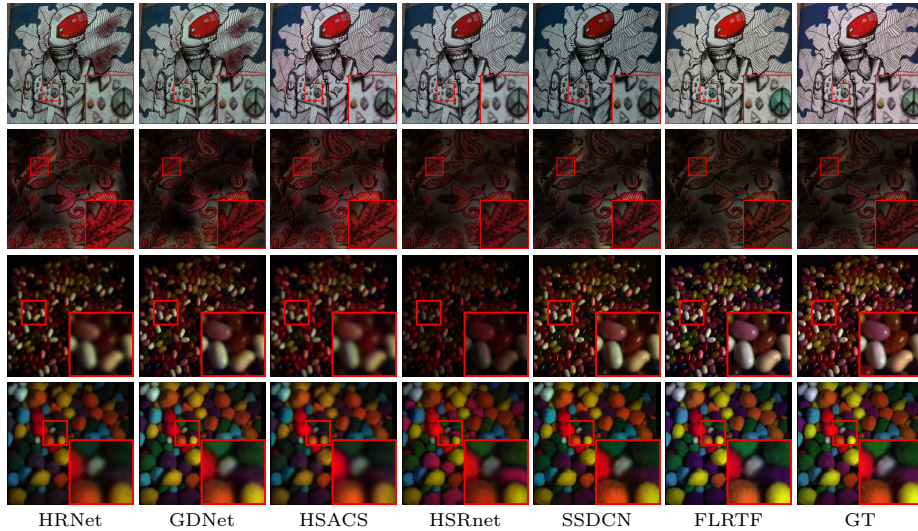


Fig. 4: Visualization of recovery results by various methods in MSSR task. From top to bottom: *ARAD_1K_912* (R:31, G:15, and B:10) and *ARAD_1K_928* (R:31, G:18, and B:10) provided by *ARAD_1K* dataset, and *Jelly Beans* (R:31, G:15, and B:5) and *Pompoms* (R:31, G:15, and B:5) provided by *CAVE* dataset.

Table 4: Quantitative comparison of different methods for MSSR task. The best and second-best values are highlighted in bold and underline, respectively.

Data	<i>ARAD_1K</i>			<i>CAVE</i>		
Method	PSNR \uparrow	SSIM \uparrow	SAM \downarrow	PSNR \uparrow	SSIM \uparrow	SAM \downarrow
HRNet	26.730	0.8872	<u>6.210</u>	23.305	0.7551	<u>35.335</u>
GDNet	28.348	0.8885	8.133	26.251	0.7821	37.443
HSACS	<u>33.269</u>	<u>0.9478</u>	6.050	23.591	0.7611	35.587
HSRnet	30.762	0.9190	7.392	20.401	0.7082	37.011
SSDCN	26.318	0.8483	8.166	<u>26.963</u>	<u>0.7952</u>	38.443
FLRTF	40.600	0.9760	6.914	35.327	0.9349	27.225

we resize them into $256 \times 256 \times 31$ for our experiments. For *ARAD_1K* dataset, which covers the wavelength range from 400 nm to 700 nm and contains 1000 scenarios, we select 901 to 950 scenarios as testing data. The size of all data is $482 \times 512 \times 31$. To comprehensively evaluate the proposed FLRTF, we compare it with five classic deep learning-based spectral super-resolution algorithms, including HRNet [51], GDNet [55], HSACS [22], HSRnet [9], and SSDCN [9].

4.3 Experimental Results

Video Frame Synthesis. Table 2 presents the quantitative evaluation metrics of the recovered results achieved by different methods for video frame syn-

thesis. Especially, we highlight the best and second-best results by bold and underlined, respectively. Generally, TNN-3DTV achieves the second-best performance for video frame interpolation, while HLRTF achieves the second-best results for video frame extrapolation. Our proposed method, *i.e.*, FLRTF, consistently outperforms the compared methods under nearly all scenarios. This improvement can be attributed to the functional transform that allows FLRTF to simultaneously exploit local smoothness of multi-dimensional data in the temporal/spectral dimensional and its global low-rankness.

To visually compare the recovered results, we present the results obtained by different methods for video frame synthesis in Fig. 2. From Fig. 2, we can observe that the proposed FLRTF achieves superior visual results compared to other methods in both the restoration of global structure and preservation of local details. Specifically, the recovered results obtained by TNN-3DTV and t-CTV contain a large number of artifacts, while DCTNN and HLRTF cannot accurately recover local details, especially in facial regions.

MSI Band Interpolation. Quantitative evaluation metrics of the recovered results obtained by different methods for MBI task are given in Table 3. We can observe that the proposed FLRTF consistently outperforms the compared methods across all datasets. More precisely, the proposed FLRTF achieves an average PSNR gain of approximately 6 dB over the second-best methods. To further analyze the performance of spectral curve recovery, Fig. 3 illustrates the spectral curves at one spatial location of the recovered results by different methods. We can observe that the spectral curves obtained by FLRTF better approximate the original one compared to those from other methods. These observations demonstrate the superior performance of the proposed FLRTF in recovering spatial images and preserving spectral signatures compared to other methods.

MSI Spectral Super-Resolution. The quantitative evaluation metrics of recovery results achieved by various methods for MSSR task are reported in Table 4. As we can see, the suggested FLRTF achieves the best PSNR, SSIM, and SAM values. Fig. 4 illustrates the false-color restoration results by various methods on *ARAD_1K* and *CAVE* datasets. From Fig. 4, we can observe that the recovered results obtained by the proposed FLRTF exhibit clearer spatial details and textures, and colors are closer to the original ones.

4.4 Discussions

Functional Transform *vs.* Discrete Transform. To validate the effectiveness of the functional transform, we compare FLRTF with two classical discrete transform-based low-rank tensor factorization methods, *i.e.*, the discrete Fourier transform-based LRTF (*i.e.*, TCTF [54]) and the deep learning-based LRTF (*i.e.*, HLRTF [29] without parametric total variation regularization). Fig. 5 illustrates the recovery results by different methods. We can observe that FLRTF achieves good restoration result, whereas other methods cannot recover the missing bands. This success is attributed to the continuity introduced by

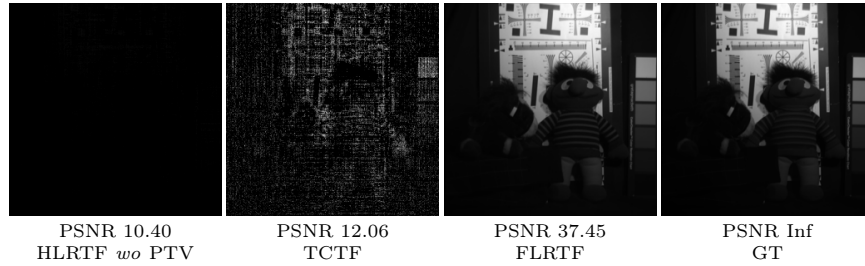


Fig. 5: Visualization of recovery results by different methods for MBI task on *Toy*.

Table 5: The performance of different methods.

Method	<i>Apply Eye Make-up</i>	<i>Blowing Candles</i>	<i>Writing On Board</i>	<i>Typing</i>
LRTFR	31.16/0.939	29.64/0.888	28.17/0.910	30.79/0.908
FLRTF	32.83/0.954	31.10/0.915	28.86/0.913	31.94/0.931

the functional transform, which enables FLRTF to capture the local smoothness of data, thereby facilitating the recovery of temporal/spectral degeneration problems.

Comparison with LRTFR [28]. The t-SVD serves as a core building block in the proposed FLRTF. The suggested functional transform-based low-rank tensor factorization can break the limitation of discrete transforms and inherits classic discrete transform-based t-SVD’s nice ability. Here, we compare the proposed FLRTF with the low-rank tensor function representation (LRTFR) [28], which introduces the functional representation into the Tucker decomposition. The recovery results by different methods are given in Table 5. The results shown in Table 5 demonstrate the superiority of our method over LRTFR.

5 Conclusion

In this paper, we proposed a novel approach, termed FLRTF, which is designed to address the challenging multi-dimensional data recovery, *i.e.*, temporal/spectral degeneration scenarios. We theoretically justified that the proposed FLRTF can encode the local smoothness and global low-rankness of data simultaneously. Extensive experiments have validated the superiority of the proposed FLRTF compared to representative data recovery methods. This work will contribute to advancing the field of computer vision and pattern recognition.

Acknowledgments: This research is supported by NSFC (Grant Nos. 62306248, 12371456, 12171072, 62131005), Sichuan Science and Technology Program (Grant Nos. 2024NSFJQ0038, 2023ZYD0007), Postdoctoral Fellowship Program of CPSF (Grant No. GZC20232197), National Key Research and Development Program of China (Grant No. 2020YFA0714001), and Fundamental Research Funds for the Central Universities (Grant No. A0920502052301-181).

References

1. Bengua, J.A., Phien, H.N., Tuan, H.D., Do, M.N.: Efficient tensor completion for color image and video recovery: Low-rank tensor train. *IEEE Transactions on Image Processing* **26**(5), 2466–2479 (2017)
2. Braman, K.: Third-order tensors as linear operators on a space of matrices. *Linear Algebra and its Applications* **433**(7), 1241–1253 (2010)
3. Cao, F., Cai, M., Tan, Y.: Image interpolation via low-rank matrix completion and recovery. *IEEE Transactions on Circuits and Systems for Video Technology* **25**(8), 1261–1270 (2015)
4. Cao, X., Lian, Y., Wang, K., Ma, C., Xu, X.: Unsupervised hybrid network of transformer and CNN for blind hyperspectral and multispectral image fusion. *IEEE Transactions on Geoscience and Remote Sensing* **62**, Art no. 5507615 (2024)
5. Chen, X., Lei, M., Saunier, N., Sun, L.: Low-rank autoregressive tensor completion for spatiotemporal traffic data imputation. *IEEE Transactions on Intelligent Transportation Systems* **23**(8), 12301–12310 (2022)
6. Dao, M., Suo, Y., Chin, S., Tran, T.: Video frame interpolation via weighted robust principal component analysis. In: 2013 IEEE International Conference on Acoustics, Speech and Signal Processing. pp. 1404–1408 (2013)
7. Dolgov, S., Kalise, D., Saluzzi, L.: Data-driven tensor train gradient cross approximation for hamilton–jacobi–bellman equations. *SIAM Journal on Scientific Computing* **45**(5), 2153–2184 (2023)
8. Hang, R., Liu, Q., Li, Z.: Spectral super-resolution network guided by intrinsic properties of hyperspectral imagery. *IEEE Transactions on Image Processing* **30**, 7256–7265 (2021)
9. He, J., Li, J., Yuan, Q., Shen, H., Zhang, L.: Spectral response function-guided deep optimization-driven network for spectral super-resolution. *IEEE Transactions on Neural Networks and Learning Systems* **33**(9), 4213–4227 (2022)
10. He, J., Yuan, Q., Li, J., Xiao, Y., Liu, D., Shen, H., Zhang, L.: Spectral super-resolution meets deep learning: Achievements and challenges. *Information Fusion* **97**, 101812 (2023)
11. He, Y., Atia, G.K.: Robust low-tubal-rank tensor completion based on tensor factorization and maximum correntopy criterion. *IEEE Transactions on Neural Networks and Learning Systems* (2023). <https://doi.org/10.1109/TNNLS.2023.3280086>
12. Hou, J., Zhang, F., Qiu, H., Wang, J., Wang, Y., Meng, D.: Robust low-tubal-rank tensor recovery from binary measurements. *IEEE Transactions on Pattern Analysis and Machine Intelligence* **44**(8), 4355–4373 (2022)
13. Jiang, H., Sun, D., Jampani, V., Yang, M.H., Learned-Miller, E., Kautz, J.: Super slo-mo: High quality estimation of multiple intermediate frames for video interpolation. In: 2018 IEEE/CVF Conference on Computer Vision and Pattern Recognition. pp. 9000–9008 (2018)

14. Jiang, T.X., Ng, M.K., Zhao, X.L., Huang, T.Z.: Framelet representation of tensor nuclear norm for third-order tensor completion. *IEEE Transactions on Image Processing* **29**, 7233–7244 (2020)
15. Jiang, T.X., Zhao, X.L., Zhang, H., Ng, M.K.: Dictionary learning with low-rank coding coefficients for tensor completion. *IEEE Transactions on Neural Networks and Learning Systems* **34**(2), 932–946 (2023)
16. Jiang, W., Zhang, J., Zhang, C., Wang, L., Qi, H.: Robust low tubal rank tensor completion via factor tensor norm minimization. *Pattern Recognition* **135**, 109169 (2023)
17. Kilmer, M.E., Horesh, L., Avron, H., Newman, E.: Tensor-tensor algebra for optimal representation and compression of multiway data. *Proceedings of the National Academy of Sciences* **118**(28) (2021)
18. Kingma, D., Ba, J.: Adam: A method for stochastic optimization. in *International Conference on Learning Representations (ICLR)* (2015)
19. Kolda, T.G., Bader, B.W.: Tensor decompositions and applications. *SIAM Review* **51**(3), 455–500 (2009)
20. Kong, H., Lu, C., Lin, Z.: Tensor Q-rank: New data dependent tensor rank. *Machine Learning* **10**, 1867–1900
21. Kong, W., Zhang, F., Qin, W., Feng, Q., Wang, J.: Low-tubal-rank tensor completion via local and nonlocal knowledge. *Information Sciences* **657**, 120002 (2024)
22. Li, J., Wu, C., Song, R., Li, Y., Xie, W., He, L., Gao, X.: Deep hybrid 2-D–3-D CNN based on dual second-order attention with camera spectral sensitivity prior for spectral super-resolution. *IEEE Transactions on Neural Networks and Learning Systems* **34**(2), 623–634 (2023)
23. Liu, J., Musialski, P., Wonka, P., Ye, J.: Tensor completion for estimating missing values in visual data. *IEEE Transactions on Pattern Analysis and Machine Intelligence* **35**(1), 208–220 (2013)
24. Liu, Y., Ng, M.K.: Deep neural network compression by tucker decomposition with nonlinear response. *Knowledge-Based Systems* **241**, 108171 (2022)
25. Lu, C., Feng, J., Chen, Y., Liu, W., Lin, Z., Yan, S.: Tensor robust principal component analysis with a new tensor nuclear norm. *IEEE Transactions on Pattern Analysis and Machine Intelligence* **42**(4), 925–938 (2020)
26. Lu, C., Peng, X., Wei, Y.: Low-rank tensor completion with a new tensor nuclear norm induced by invertible linear transforms. In: *2019 IEEE/CVF Conference on Computer Vision and Pattern Recognition (CVPR)*. pp. 5989–5997 (2019)
27. Luo, Y.S., Zhao, X.L., Jiang, T.X., Chang, Y., Ng, M.K., Li, C.: Self-supervised nonlinear transform-based tensor nuclear norm for multi-dimensional image recovery. *IEEE Transactions on Image Processing* **31**, 3793–3808 (2022)
28. Luo, Y., Zhao, X., Li, Z., Ng, M.K., Meng, D.: Low-rank tensor function representation for multi-dimensional data recovery. *IEEE Transactions on Pattern Analysis and Machine Intelligence* **46**(5), 3351–3369 (2024)
29. Luo, Y., Zhao, X., Meng, D., Jiang, T.: HLRTF: Hierarchical low-rank tensor factorization for inverse problems in multi-dimensional imaging. In: *2022 IEEE/CVF Conference on Computer Vision and Pattern Recognition (CVPR)*. pp. 19281–19290 (2022)
30. Madathil, B., George, S.N.: DCT based weighted adaptive multi-linear data completion and denoising. *Neurocomputing* **318**, 120–136 (2018)
31. Mishra, K.V., Cho, M., Kruger, A., Xu, W.: Spectral super-resolution with prior knowledge. *IEEE Transactions on Signal Processing* **63**(20), 5342–5357 (2015)

32. Peng, J., Wang, Y., Zhang, H., Wang, J., Meng, D.: Exact decomposition of joint low rankness and local smoothness plus sparse matrices. *IEEE Transactions on Pattern Analysis and Machine Intelligence* **45**(5), 5766–5781 (2023)
33. Purushwalkam, S., Ye, T., Gupta, S., Gupta, A.: Aligning videos in space and time. In: *Computer Vision – ECCV 2020*. pp. 262–278 (2020)
34. Qiu, D., Bai, M., Ng, M.K., Zhang, X.: Robust low-rank tensor completion via transformed tensor nuclear norm with total variation regularization. *Neurocomputing* **435**, 197–215 (2021)
35. Rout, L.: Alert: Adversarial learning with expert regularization using tikhonov operator for missing band reconstruction. *IEEE Transactions on Geoscience and Remote Sensing* **58**(6), 4395–4405 (2020)
36. Shao, P., Zhang, D., Yang, G., Tao, J., Che, F., Liu, T.: Tucker decomposition-based temporal knowledge graph completion. *Knowledge-Based Systems* **238**, 107841 (2022)
37. Siyao, L., Zhao, S., Yu, W., Sun, W., Metaxas, D., Loy, C.C., Liu, Z.: Deep animation video interpolation in the wild. In: *Proceedings of the IEEE/CVF Conference on Computer Vision and Pattern Recognition (CVPR)*. pp. 6587–6595 (June 2021)
38. Tang, X., Hu, X., Gu, X., Sun, J.: Residual-conditioned optimal transport: Towards structure-preserving unpaired and paired image restoration. In: *Forty-first International Conference on Machine Learning (2024)*, <https://openreview.net/forum?id=irBHP1kxP>
39. Tang, X., Zhao, X., Liu, J., Wang, J., Miao, Y., Zeng, T.: Uncertainty-aware unsupervised image deblurring with deep residual prior. In: *Proceedings of the IEEE/CVF Conference on Computer Vision and Pattern Recognition (CVPR)*. pp. 9883–9892 (June 2023)
40. Thanh, L.T., Abed-Meraim, K., Trung, N.L., Hafiane, A.: Robust tensor tracking with missing data and outliers: Novel adaptive CP decomposition and convergence analysis. *IEEE Transactions on Signal Processing* **70**, 4305–4320 (2022)
41. Vervliet, N., Debals, O., Lathauwer, L.D.: Exploiting efficient representations in large-scale tensor decompositions. *SIAM Journal on Scientific Computing* **41**(2), A789–A815 (2019)
42. Wang, H., Peng, J., Qin, W., Wang, J., Meng, D.: Guaranteed tensor recovery fused low-rankness and smoothness. *IEEE Transactions on Pattern Analysis and Machine Intelligence* **45**(9), 10990–11007 (2023)
43. Wang, J.L., Huang, T.Z., Zhao, X.L., Jiang, T.X., Ng, M.K.: Multi-dimensional visual data completion via low-rank tensor representation under coupled transform. *IEEE Transactions on Image Processing* **30**, 3581–3596 (2021)
44. Wang, J.L., Zhao, X.L., Li, H.C., Cao, K.X., Miao, J., Huang, T.Z.: Unsupervised domain factorization network for thick cloud removal of multitemporal remotely sensed images. *IEEE Transactions on Geoscience and Remote Sensing* **61**, **Art no. 5405912** (2023)
45. Wang, W., Aggarwal, V., Aeron, S.: Efficient low rank tensor ring completion. In: *Proceedings of the IEEE International Conference on Computer Vision (ICCV)* (Oct 2017)
46. Wang, X., Yang, L.T., Wang, Y., Ren, L., Deen, M.J.: ADTT: A highly efficient distributed tensor-train decomposition method for IIoT big data. *IEEE Transactions on Industrial Informatics* **17**(3), 1573–1582 (2021)
47. Wang, Y., Li, W., Liu, N., Gui, Y., Tao, R.: Fubay: An integrated fusion framework for hyperspectral super-resolution based on bayesian tensor ring. *IEEE Transactions on Neural Networks and Learning Systems* (2023). <https://doi.org/10.1109/TNNLS.2023.3281355>

48. Zeng, C., Jiang, T.X., Ng, M.K.: An approximation method of CP rank for third-order tensor completion. *Numerische Mathematik* **147**(3), 727–757 (2021)
49. Zhang, Z., Aeron, S.: Exact tensor completion using t-SVD. *IEEE Transactions on Signal Processing* **65**(6), 1511–1526 (2017)
50. Zhao, X.L., Zhang, H., Jiang, T.X., Ng, M.K., Zhang, X.J.: Fast algorithm with theoretical guarantees for constrained low-tubal-rank tensor recovery in hyperspectral images denoising. *Neurocomputing* **413**, 397–409 (2020)
51. Zhao, Y., Po, L.M., Yan, Q., Liu, W., Lin, T.: Hierarchical regression network for spectral reconstruction from RGB images. In: 2020 IEEE/CVF Conference on Computer Vision and Pattern Recognition Workshops (CVPRW). pp. 1695–1704 (2020)
52. Zheng, Y.B., Huang, T.Z., Zhao, X.L., Zhao, Q.: Tensor completion via fully-connected tensor network decomposition with regularized factors. *Journal of Scientific Computing* **92**(8) (2022)
53. Zheng, Y.B., Huang, T.Z., Zhao, X.L., Zhao, Q., Jiang, T.X.: Fully-connected tensor network decomposition and its application to higher-order tensor completion. *Proceedings of the AAAI Conference on Artificial Intelligence* **35**(12), 11071–11078 (2021)
54. Zhou, P., Lu, C., Lin, Z., Zhang, C.: Tensor factorization for low-rank tensor completion. *IEEE Transactions on Image Processing* **27**(3), 1152–1163 (2018)
55. Zhu, Z., Liu, H., Hou, J., Jia, S., Zhang, Q.: Deep amended gradient descent for efficient spectral reconstruction from single RGB images. *IEEE Transactions on Computational Imaging* **7**, 1176–1188 (2021)